International Journal of Fatigue 168 (2023) 107411

Contents lists available at ScienceDirect

International Journal of Fatigue

journal homepage: www.elsevier.com/locate/ijfatigue

On the effect of environmental temperature on fracture fatigue entropy

Mohammad A. Amooie, M.M. Khonsari *

Department of Mechanical and Industrial Engineering, Louisiana State University, Baton Rouge, LA 70803, United States

ARTICLE INFO

Keywords:
Fracture fatigue entropy
Internal friction
Low-temperature fracture
Bending fatigue tests
Irreversible thermodynamics

ABSTRACT

Fracture behavior of carbon steel 1018 operating in low-temperature environments is investigated. Specifically, fully-reversed bending experimental tests are performed to examine the efficacy of applying the concept of Fracture Fatigue Entropy (FFE) for predicting fatigue life at different environmental temperatures. A large cooling chamber was constructed that houses the entire bending test rig and maintains the environmental temperature at the desired value down to −10 °C. It is shown that under conditions tested, fatigue life improves at lower operating temperatures. Results also reveal that FFE remains nearly constant and can be used for reliable prediction of fatigue life. Illustrative examples are provided to show the utility of the approach for prediction purposes.

1. Introduction

Metal fatigue presents a major concern for safety and maintenance practices in industry [1–3]. Of particular interest in both the design and health monitoring of components is a reliable prediction of fatigue life under specific working conditions. While rich volumes of research data are available in the open literature, a general method capable of predicting how environmental temperature affects fatigue life is lacking [4].

A notable early work (1957) on low-temperature fatigue is by McCammon and Rosenberg [5], who performed cyclic tension–compression experiments at temperatures between −269 °C to 20 °C and calculated fatigue life for copper, silver, gold, aluminum, magnesium, zinc and iron. They showed that, except in the case of iron and zinc, the fatigue characteristics of these materials improved considerably at low temperatures. Stephens et al. [6] in 1979 presented a review of the impact of low-temperature environments on the fatigue life of different types of steel, such as carbon steel, cast steel, etc. They showed that at low temperatures, the fatigue resistance of unnotched and notched specimens improved, and fatigue life in high-cycle fatigue tests increased; however, this change was found to be more pronounced in unnotched specimens. At low-cycle fatigue tests different behaviors were observed for various steels. Low ductility and low fracture toughness are two important factors in lower temperatures.

Verkin et al. [7] in 1983 published a review article on the influence of low-temperature environments on the fatigue life of metals and alloys. They attempted to analyze the effect of low temperatures on the rate of crack growth via linear fracture mechanics and introduced Equation (1) to describe the crack propagation rate in high-strength steels for temperatures between 20 °C and −100 °C.

$$\frac{dl}{dN} = Aexp\left(\frac{-U_0 + aln(\Delta K)}{RT}\right) \tag{1}$$

where U_0 is the initiation energy, ΔK is the difference between the initial threshold and critical stresses, A and a are material constants, R is the universal gas constant and T is temperature. They observed that crack nucleation at low temperatures takes longer to develop since the planar slip of dislocations increases; however, once formed, the crack growth rate is faster than at room temperature.

Vogt et al. [8], in 1991, investigated the effect of low temperature and nitrogen alloying for 316L-type austenitic stainless steel. The results revealed that adding nitrogen to the specimen increases fatigue resistance at both 27 °C and −196 °C. Low-cycle fatigue tests also exhibited an increase in planar slip of dislocations, confirming the increase in fatigue life at lower temperatures for such materials. Kang et al. [9] in 2009 experimentally investigated the impact of low temperatures on the static and fatigue behavior of welded SM490A steel. The results of the study showed that, down to −40 °C, the static strength of the material increased and the fatigue life improved. However, the improvement was found to be significantly dependent on welding the material.

In 2013 Fassina et al. [10] conducted tests on X65 micro-alloyed and F22 low alloy steels embrittled with hydrogen at various temperatures and frequencies. The results show that although reference [7] suggests that temperature and crack propagation have opposite relations for

---

* Corresponding author.
E-mail address: khonsari@lsu.edu (M.M. Khonsari).

https://doi.org/10.1016/j.ijfatigue.2022.107411
Received 6 October 2022; Received in revised form 17 November 2022; Accepted 20 November 2022
Available online 24 November 2022

high-strength steels, hydrogen embrittlement can change this behavior. This means that an increase in temperature between room temperature and the minimum of −100 °C increases the crack growth rate. Jung et al. [11] in 2014 investigated how low temperatures could affect the fatigue crack propagation in X80 steel. A drastic reduction in crack propagation rate was found in lower temperatures. Liao et al. [12] experimentally investigated the crack propagation rate and its dependency on low ambient temperature influences the rate for Q345qD steel, typically used in bridge constructions in China. Their results showed that the crack growth rate in the base material decreased by reducing the temperature to −60 °C; however, the opposite was found for the butt welds. They attributed this behavior to the lower ductile-to-brittle transition temperature in the base material, where the weld metal exhibited the opposite trend. Zhang et al. [13] used Q420 steel to study modifications caused by lower environmental temperatures on fatigue strength. Their experimental data also revealed that the life improves with a decrease in temperature in such material.

While a host of empirical results are available on the effect of temperature on fatigue life, they are largely limited to specific operating conditions and lack generalization. Recent efforts in applying the principles of irreversible thermodynamics show that it is possible to develop a general framework for treating mechanical fatigue [14]. In particular, research shows that the concept of Fracture Fatigue Entropy (FFE) introduced by Naderi et al. [15] provides a general fatigue degradation index applicable to different loading and operating conditions. FFE is the cumulative entropy generated during the fatigue process beyond which fracture occurs. Extensive research shows that the FFE does not depend on the geometry or the type of loading, tension–compression, torsion, or bending and can be viewed as a material property. The efficacy of FFE has been experimentally validated by Jang and Khonsari [16]. Jirandehi and Khonsari [17] presented a microstructure-sensitive model for the evaluation of dissipated energy for Al 7075-T6 and LCS 1018. The data generated using an FEM showed good agreement with measured FFE using an IR camera. Teng et al. [18] experimentally validated FFE for SAE 1045 and showed that the FFE is an independent parameter from loading amplitudes. In 2016 Ontiveros et al. [19] also investigated the validity of FFE for predicting crack initiation of AA7075-T651 notched specimens. Results were obtained using hysteresis loops and measuring surface temperature evolution. Idris et al. [20] used entropy generation during a fatigue process to investigate the crack propagation rate. The FFE concept has also been employed to predict life and S-N curves for carbon fiber reinforced polymer by Huang et al. [21], who should that FFE is independent of stress amplitudes for such polymers. In 2021 Wei et al. [22] used FFE to study the fatigue behavior of Q460 welded joints for high-cycle fatigue and showed that the results for predicting fatigue limit are consistent with the traditional staircase method. A recent work by Huang et al. [23] extends the applications of FFE to life evaluation for carbon-based composite materials. The results suggest FFE on logarithmic scale experiences no difference under various loading stresses.

The first investigation on the effect of environmental temperature on FFE was conducted by Haghshenas and Khonsari [24]. They built an environmentally-controlled heating chamber and performed fully-reversed bending tests on carbon steel 1018 specimens from 20 °C to 200 °C. They showed that under the conditions tested, the fatigue life decreased as the environmental temperature increased. However, the average FFE remained relatively constant. More recently, Jirandehi et al. [4] presented experimental and computation results for FFE of additively manufactured C-1815 copper alloy specimens up to 426 °C in tension–compression mode and reported that the average FFE remains constant.

This paper investigates the applicability of FFE in low environmental temperatures. The outline of this paper is as follows. The background formulation of FFE, the governing equations, and the concept of internal friction as a non-damaging parameter are presented in Section 2. The third section describes the material specifications and preparation techniques. Section 4 is devoted to the testing machine, test environment, sensors and experimental procedure, and Section 5 discusses the results of the room and low-temperature fatigue tests. Section 6 presents the applications of FFE for life prediction with experimental verification. The summary and concluding remarks are covered in Section 7.

2. Theory

2.1. Fracture fatigue entropy

The first law of thermodynamics states that the rate of change in the internal energy of a control volume is equal to the rate of work done through the control volume added to the rate of heat transfer associated with that control volume. This law can be applied to a control volume containing any type of structure undergoing time-dependent cyclic stress or strain. As the material inside the control volume experiences plastic and inelastic deformation due to work done via external actuation, internal heat generation causes the material to experience self-heating.

$$\int_V \dot{E}_g dV + \int_V k\nabla^2 T dV - \int_{A_{gs}} h(T-T_\infty)dA - \int_{A_{gs}} \varepsilon\sigma_n(T^4 - T_\infty^4)dA = \int_V \rho C_p \frac{\partial T}{\partial t} dV \tag{2}$$

where $\dot{E}_g$ is the generated energy due to plastic strain, and the thermal conductivity, heat transfer coefficient, emissivity and Stefan-Boltzmann coefficients are denoted as k, h, ε, and σ_n , respectively, and A_{gs} stands for gage surface area. Assuming that $\dot{E}_g$ is the mechanical energy into the control volume and considering a uniform gage section equation (3) can be written [25].

$$k\frac{\partial^2 T}{\partial X^2} - \frac{hP}{A_{gs}}(T-T_a) - \frac{\varepsilon\sigma_n P}{A_{gs}}\left(T^4 - T_a^4\right) + \dot{E}_g = \rho C_p \frac{\partial T}{\partial t} \tag{3}$$

where T_a is the ambient temperature and P is the perimeter. Considering the temperatures in Kelvin, the temperature difference is generally negligible compared to ambient temperature. Letting $\theta = T - T_a$, and $\dot{E}_g$ to be $\dot{w}_p$, and linearizing the radiation term using Taylor series, Equation (4) will be obtained.

$$\frac{\partial^2\theta}{\partial X^2} - m^2\theta + \dot{W}_p = \frac{1}{\alpha}\frac{\partial\theta}{\partial t} \tag{4}$$

where α is the diffusivity, and $m^2 = \frac{(h+4\varepsilon\sigma_n T_a^3)P}{Ak}$. The second order differential equation can be solved considering homogenous and equilibrium solution. The final derivative for θ is shown in equation (5). The interested reader may refer to reference [25] for complete derivation.

$$\frac{d\theta}{dt} = -2\alpha\frac{\dot{W}_p}{m^2 k}\sum_{n=1}^{\infty} C_n\left[\left(\frac{n\pi}{L}\right)^2 + m^2\right]\sin\left(\frac{n\pi}{L}X\right)e^{-\left[\left(\frac{n\pi}{L}\right)^2 + m^2\right]\alpha t} \tag{5}$$

Where L is the boundary length of the control volume and C_n is defined in equation (6). Time derivative of θ at t = 0 will result in equation (Eqn 7).

$$C_n = -\left[\frac{1}{n\pi} - \frac{n\pi}{(n\pi)^2 + L^2 m^2}\right]\left[1-(-1)^n\right] \tag{6}$$

$$R_\theta = \frac{2\dot{W}_p}{\pi\rho C_p}\sum_{n=1}^{\infty}\left[\frac{1-(-1)^n}{n}\right]\sin\left(\frac{n\pi}{2}\right) = \frac{4\dot{W}_p}{\pi\rho C_p}\sum_{n=1}^{\infty}\left[\frac{1-(-1)^n}{n}\right] = \frac{\dot{W}}{\rho C_p} \tag{7}$$

Therefore,

$$W_p = \rho C_p R_\theta \tag{8}$$

The second law of thermodynamics in terms of Clasius-Duhem inequality is stated below.

$$\rho\dot{\eta} \geq -\nabla.\left(\frac{q}{T}\right)+\frac{\rho s}{T} \tag{9}$$

where ρ is the mass density, $\dot{\eta}$ is the rate of entropy per unit mass, q is the heat flux vector, T denotes the absolute temperature and s represents an energy source per unit mass [26].

$$\dot{\eta} = \frac{W_p}{T} - \frac{J_q.\nabla T}{T^2} - \frac{\dot{E}}{T} \geq 0 \tag{12}$$

where J_q is the conductive heat flux. The entropy due non-recoverable energy stored in the material can be neglected [27]. Therefore, $\frac{\dot{E}}{T}$ can be assumed negligible.

As seen in Equation (12), entropy generation depends on two factors: the dissipated energy due to plastic deformation and heat conduction. Naderi et al. [15] showed that the entropy generation related to heat conduction is insignificant and can be neglected. Thus Equation (12) simplifies to.

$$\dot{\eta} = \frac{W_p}{T} \tag{13}$$

By integrating the above equation over the time in which the fatigue process takes place, the accumulated produced entropy can be predicted.

$$\eta = \int_0^t \frac{W_p}{T} dt \tag{14}$$

FFE can be determined by integrating Equation (14) to t_f, the time at fracture occurs, with N_f as the associated number of cycles to failure.

$$\mathrm{FFE} = \eta = \int_0^{t_f} \frac{W_p}{T} dt = \frac{W_p}{T} \times \frac{N_f}{f} \tag{15}$$

where f is the actuation frequency.

Equation (15) implies that if the FFE of a material is known, one can predict the fatigue life N_f. This requires one to evaluate W_p and T. Therefore, accumulated entropy generation through the process can be acquired by the following relation.

$$\mathrm{FFE} = \frac{\rho C_p R_\theta}{T} \times \frac{N_f}{f} \tag{16}$$

where R_θ is the rate of temperature variations at the beginning of the operation. See Fig. 1.

Thus, FFE can be evaluated by measuring the temperature rise at the beginning of the experiment. An alternative approach for determining R_θ is to halt the experiment after reaching a steady state (Phase II) and then measuring the rate at which the specimen cools [28]. It can be shown that the rate at which the specimen temperature drops is precisely the same as R_θ [25].

2.2. *The role of internal friction*

Fatigue process is governed by irreversible thermodynamics in which energy dissipation due to plastic deformation progressively degrades the material until fracture. An important factor in cyclic fatigue is the so-called internal friction or anelastic energy [26], which arises when the stress or strain imparted into the structure is less than the fatigue limit (or endurance limit), and consequently the medium experiences anelastic deformation. It is worth mentioning that internal friction is studied in the context of fatigue.

In general, intrinsic defects in materials during manufacturing will turn into the shape of permanent dislocations in cyclic loadings that promotes crack initiation that grows and eventually causes fracture. Some of these substructural defects are in the form of half-planes in the material's lattice. The load imposed on the material during cyclic loading creates enough activation energy for the half-planes to experience edge dislocation. This phenomenon happens when lines of atoms in such half-planes receive enough energy to travel from neighboring energy levels, or Peirels valleys, to the next energy level. At very low-stress amplitudes, it is unlikely that all atoms receive enough energy to travel to the next Peirels valley; instead, they form kink bands that contain some of the atoms in half-planes traveling to the next Peirels valley and the rest tend to oscillate in their initial energy level. These kink bands return to their initial locations gradually and are considered to be non-damaging (Fig. 2) [4,29]. Accordingly, a material undergoing stress at levels below the fatigue limit will experience a very high number of cycles before failure. In contrast, at high-stress levels, only a small portion of half of the planes form kink bands due to a higher level of energy introduced to the material structure. Therefore, it is important to consider the share of energy dissipation that is not contributing to material degradation. Moreover, as the material receives higher amounts of energy at higher stress amplitudes, the number of local defects affected becomes greater, which means a higher number of kink bands will be formed. This will result in higher values of internal friction per cycle at larger stress levels. Generally, the value for internal friction per cycle due to anelastic deformation directly correlates with stress amplitude [30,31]. Yet, the value for accumulated energy contributed by internal friction for high-cycle tests is significantly larger than that of low-cycle fatigue tests since the anelastic deformation is multiplied by a very large

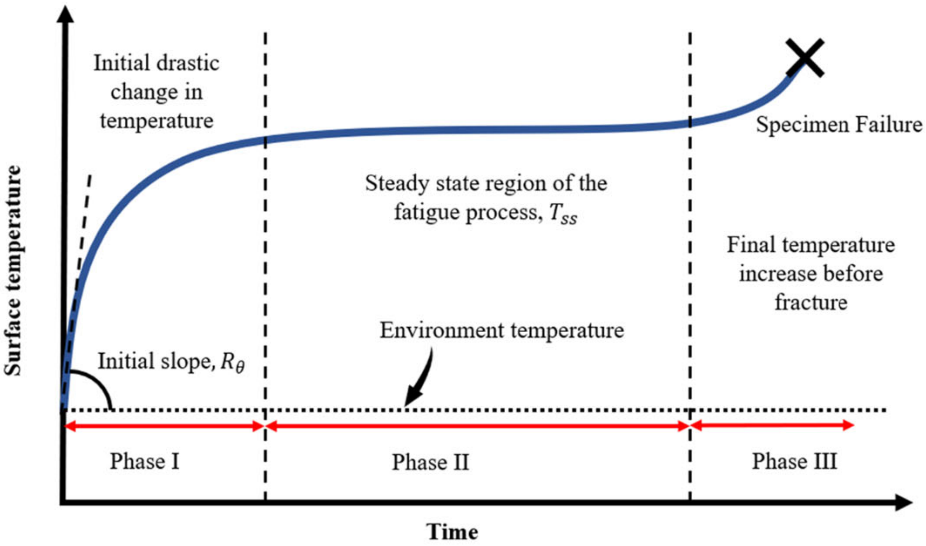

Fig. 1. Evolution of temperature.

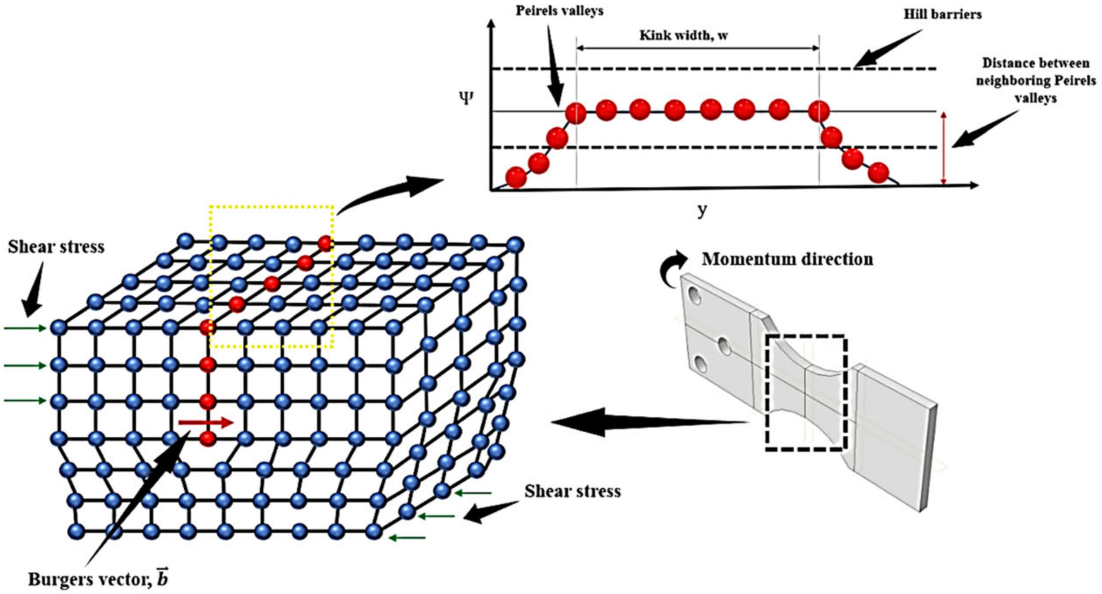

Fig. 2. Material lattice with half-planes and the direction of Burgers vector that decides the oscillatory movement of atoms between neighboring Peirles valleys. Red atoms represent the half-plane formations. Ψ is the energy level of each Hill barrier and valley and y denotes the length of half-plane in material lattice. (For interpretation of the references to colour in this figure legend, the reader is referred to the web version of this article.)

number of cycles at high and very high-cycle fatigue tests.

Fig. 3 illustrates the impact of internal friction on generated energy during fatigue process. The contribution of internal friction in dissipated energy affects the value measured for the initial slope of temperature variations. Thus, R_θ consists of two parts: one term associated with plastic deformation, R_θ^d, and the other to account for the role of internal friction, R_θ^f [26,32,33].

$$R_\theta^T = R_\theta^d + R_\theta^f \tag{17}$$

3. Material design, fabrication and preparation

Specimens are made of Carbon Steel 1018 designed for reversed bending experiments with two circular arcs on both sides to establish nominal stress alongside the test region. They were fabricated according to the American Society for Testing and Material Special Technical Publication 566 (ASTM STP 566) standards [34]. Specimens are polished longitudinally on both sides to a surface finish of 0.2 µm. Fig. 4 shows a schematic illustration of the dimensions of specimens. Table 1 and 2 show the mechanical properties and composition of CS 1018, as received by the supplier. Fig. 5 gives the stress–strain diagram for the material tested for this research.

4. Working principle of the apparatus, sensors and experimental procedure

4.1. Test apparatus

The test rig is a displacement-controlled, fully-reversed bending fatigue machine (Fatigue Dynamics, Inc.). The operator sets the desired frequency and actuation displacement and a counter keeps track of the number of cycles to failure. Fig. 6 shows a schematic illustration of the testing machine.

4.2. IR camera and thermal measurement instruments

An infrared (IR) camera (FLIR A600) with an image frequency of 50 Hz, and resolution of 640 × 480 pixels, and the capability to detect

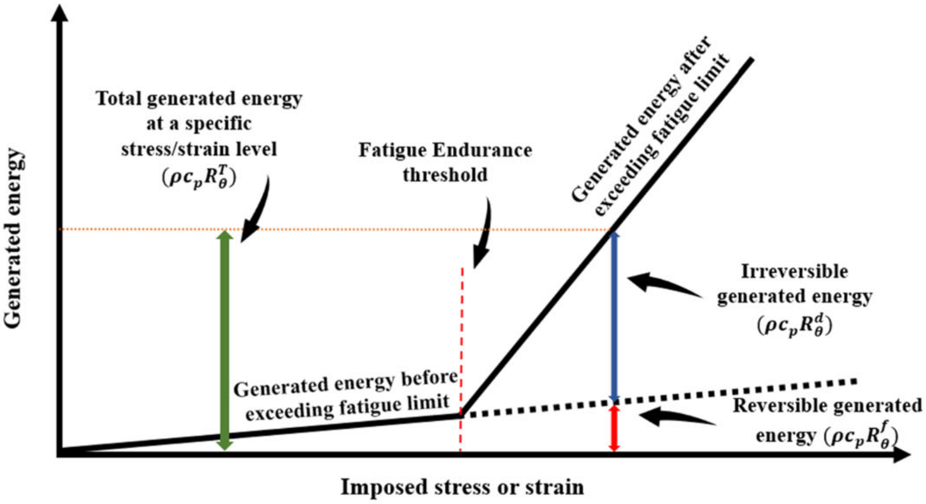

Fig. 3. Relationship between accumulated generated energy, microplastic deformation and internal friction.

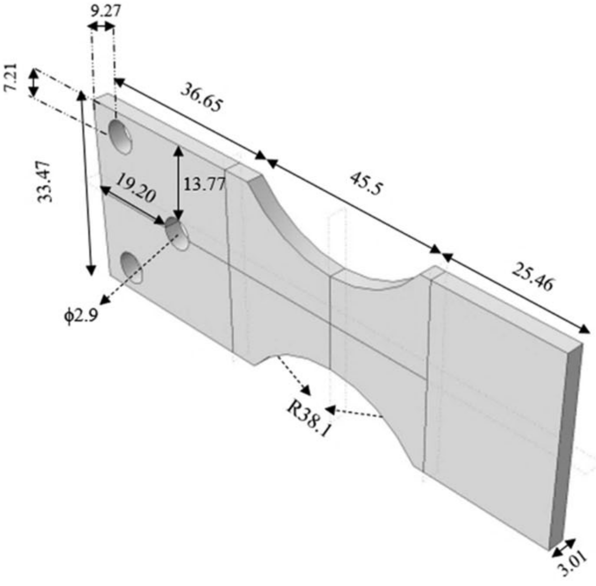

Fig. 4. Geometry and dimensions of CS 1018 specimen (all units are in mm).

temperature differences as small as 50 mK was used. The accuracy of this camera is $\pm 2^{\circ}$C or ±2% of the reading. The temperature range that the camera is capable of detecting is $-20^{\circ}C$ to 2000°C. A portable thermometer ranging from -50°C to 150°C was used to read the initial temperature inside the cooling chamber. A K-type thermocouple with a range of -50°C to 700°C was placed inside the chamber to monitor the temperature changes during the test. The design of the chamber is described next.

4.3. Cooling chamber

An insulted cooling chamber was designed and built to regulate the temperature. Its walls are made of extruded polystyrene (XPS) foam insulation (FOAMULAR 150) with a thickness of 12.7 mm. The entire test rig was placed in the cooling chamber. The bottom part of the testing table is also insulated using an insulating material. To reduce the temperature inside the box, two compact medical freezers (EdgeStar CMF151L-1) were used. The freezers are rated to reach a temperature as low as -20°C. They are placed in two different positions concerning the specimen to maintain a uniform temperature in the entire interior environment. Two fans were placed inside the freezers for air circulation to create a uniform temperature regime during the test. The chamber has two small slots for the operator to access the control box for frequency adjustments and for the IR camera to capture the specimen's surface temperature.

4.4. Stress measurement sensors

A miniature load cell (FUTEK LCM300) load cell was threaded in line with the actuator to allow assessment of the stress imparted into the specimen. To accommodate the load cell, the handle on which the load is applied had to be redesigned. A nano-volt/micro-ohm meter (KEYSIGHT 34420A) and its software (KEYSIGHT BenchVue) were utilized to register and record the output voltage of the load cell. The load captured by the loadcell is then processed to measure the stress imposed on the specimen at the point at which fracture occurs. The bending stress equation (Eq. (17)) is used to calculate the stress.

$$\sigma_{bending} = \frac{Mc}{I} \tag{18}$$

where M is the internal bending moment about the section's axis, c is the perpendicular distance from the neutral axis to the farthest point of the section, and I is the moment of inertia of the section area about the neutral axis.

4.5. Ambient and low-temperature testing

For the ambient temperature testing, the freezers are turned off until the chamber reaches room temperature. The temperature change inside the chamber remained less than 0.3 °C for all tests. The same displacement values as the low-temperature procedure were used for comparison.

For low-temperature tests, the setup is modified to provide the desired temperature by adjusting the power of the freezer. This research aims to address fatigue behavior in low-temperature environments as opposed to only locally manipulating the specimen's temperature; therefore, the entire testing rig is placed inside the cooling chamber. Thus, the minimum environmental temperature was limited to −10 °C to avoid damaging the machine's control system. Four different actuation levels have been used to capture the temperature rise on the

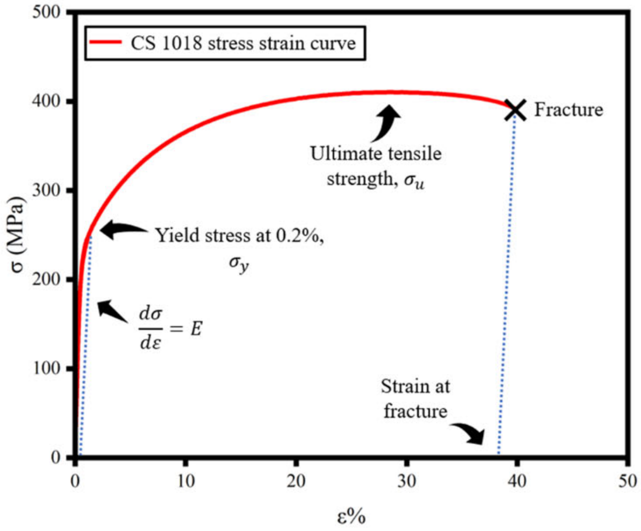

Fig. 5. Nominal stress-strain curve for tested CS 1018.

Table 1
Composition of CS 1018.

	Carbon	Manganese	Silicon	Phosphorus	Sulfur	Iron
CS 1018	0.13–0.20 %	0.30–0.90 %	0.15–0.30 %	0.04 % Max	0.50 % Max	98.06–99.42 %

Table 2
Mechanical properties of CS 1018.

	Tensile strength	Yield strength	Modulus of elasticity	Density	Poisson's ratio	Hardness, Brinell
CS 1018	398 MPa	255 MPa	205 GPa	7.86 g/cm^3	0.29	126

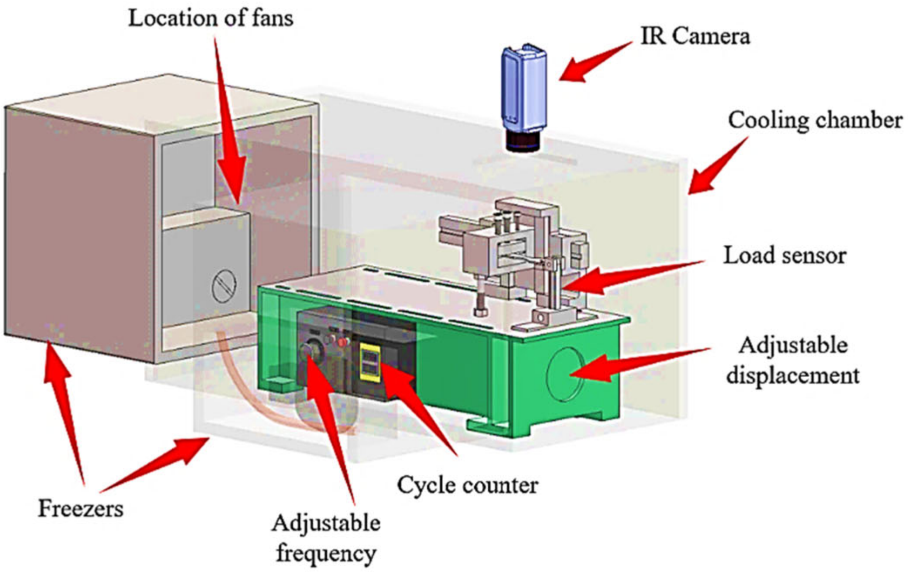

Fig. 6. Schematic bending fatigue apparatus, cooling chamber, load sensors, and IR camera.

material's surface. Note that all tests are fully reversed bending and that the displacement setting stated in this paper corresponds to half of the actuator traveling distance.

4.6. *Internal friction*

To measure the contribution of internal friction based on the environmental temperature, high-cycle fatigue tests at lower stresses were conducted at 20 °C and −10 °C. A total of 6 displacements were selected to measure the endurance limit of the specimen.

5. Results and discussion

Fig. 7 shows the measured stress amplitudes as a function of the displacement. Nonlinearity sets in when the displacement exceeds approximately 3 mm. The diagram shows for actuation values below 3 mm, the behavior is linear and elastic. This can be an indication that the actuation level is close to the endurance limit. S-N curves that include high cycle fatigue tests confirm this supposition. Fig. 8 presents the evolution of surface temperature at 6.35 mm displacement at 4 different environmental temperatures (20 °C, −6 °C, −8 °C, and −10 °C). It should be noted that the camera has the capability of capturing images of the entire surface of specimens. The images are then post-processed to get the maximum temperature from a given line at which the fracture occurs. The results show that the three-phase temperature evolution holds in all cases tested. As can be seen, the steady-state temperature is directly affected by the initial temperature rise, and the slope in which the temperature is increasing is smaller at lower temperatures, resulting in longer fatigue life (see Fig. 9).

In general, two factors alter the fracture behavior of metals at low temperatures. Typically, yield and tensile strength are improved at lower temperatures compared to those at ambient temperature. This suggests an increased ability to endure a wider range of stress without plastic deformation due to lower mobility of dislocations. The second reason for the improvement in fatigue life is that at moderately lower temperatures, the crack propagation rate slows down, particularly at a small stress concentration, ΔK, due to reduced cyclic plasticity at the crack tip [35].

Table 3 summarizes the specimen's fatigue life in 4 tested environmental temperatures. The percentage of improvement in fatigue life

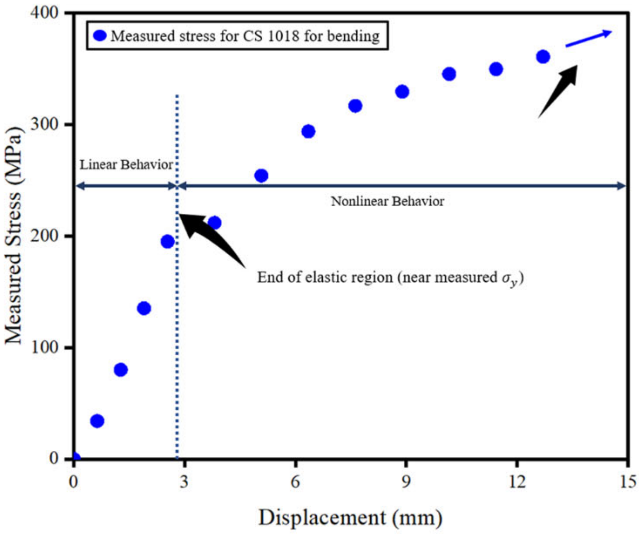

Fig. 7. Measured stress levels for different displacements with load cell.

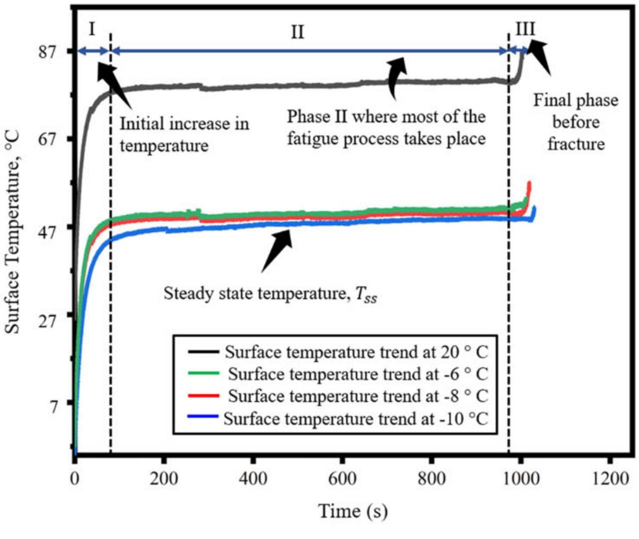

Fig. 8. Surface temperature as a function of time for 4 various temperatures for 6.35 mm displacement.

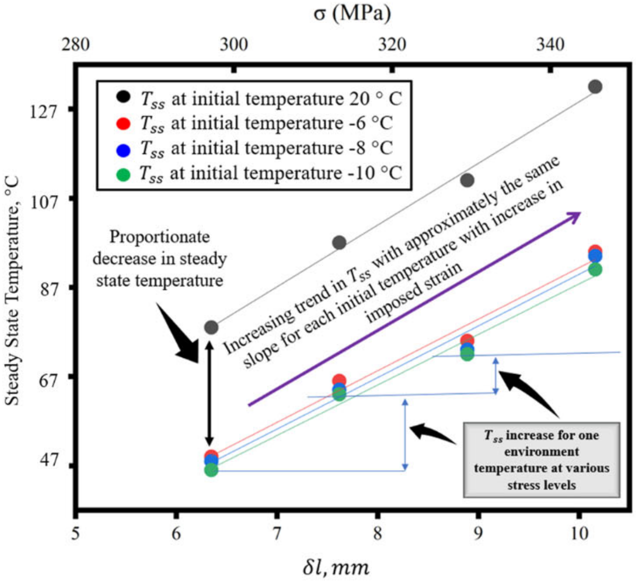

Fig. 9. Steady state temperature as a function of displacement for different initial temperatures.

depends on the imposed actuation displacement and varies from 1.59 % to 18.99 % compared to room temperature (20 °C). Under the conditions tested, the greatest improvement in fatigue life at low temperatures occurred at higher levels of imposed stress (displacement amplitudes). Data for two different temperatures at one stress level for verification are provided as well (see Table 4).

5.1. *Internal friction*

To determine the endurance limit, tests were carried out at very small displacement amplitudes, at 20 °C and −10 °C. Referring to Fig. 3, by measuring and plotting R_θ^T at various low-stress amplitudes, one would expect a linear rise in temperature below the fatigue limit. Above the fatigue limit, R_θ^T changes with increasing the stress amplitude. Fig. 10 shows the variation of R_θ^T at 20 °C for various tested displacement amplitudes. The fatigue limit and the fitted line and the internal friction contribution are presented in this figure. The same procedure is repeated at −10 °C and the results are presented in Fig. 11. As it can be seen, the internal friction equation at −10 °C has a slightly bigger slope, which means at larger displacement or stress amplitudes, the role of internal friction in measure R_θ^T is more significant. However, the accumulated dissipated energy due to internal friction for small stress amplitudes is much more appreciable. Hence, internal friction plays a much more prominent role in high-cycle fatigue. The difference in internal friction contribution per cycle at ambient and low temperatures stems from the change in enthalpy variation and activation energy needed for dislocations to experience a transition from anelastic deformation to plastic deformation since, at low temperatures, dislocation mobility is reduced.

Table 3
Life at various tested temperatures and improvement percentage compared to room temperature.

Displacement (mm)	Stress level (MPa)	Temperature (°C)	Life (Cycles)	Life improvement compared to room temperature (%)
6.35	293	20	24,700	
6.35	293	−6	25,095	1.59
6.35	293	−8	25,125	1.72
6.35	293	−10	25,194	2.00
7.62	316	20	17,120	
7.62	316	−6	18,125	5.87
7.62	316	−8	18,520	8.17
7.62	316	−10	18,670	9.05
8.89	329	20	10,600	
8.89	329	−6	12,250	15.56
8.89	329	−8	12,400	16.98
8.89	329	−10	12,430	17.26
10.16	345	20	6664	
10.16	345	−6	7880	18.24
10.16	345	−8	7896	18.48
10.16	345	−10	7930	18.99

Table 4
Data for two different temperature tests.

Environment Temperature (°C)	Stress (MPa)	Displacement (mm)	Steady-state temperature (K)	$\boldsymbol{R_\theta}\left(\frac{^\circ C}{s}\right)$
20	320	8.255	379	4.31
−10	320	8.255	341	3.45

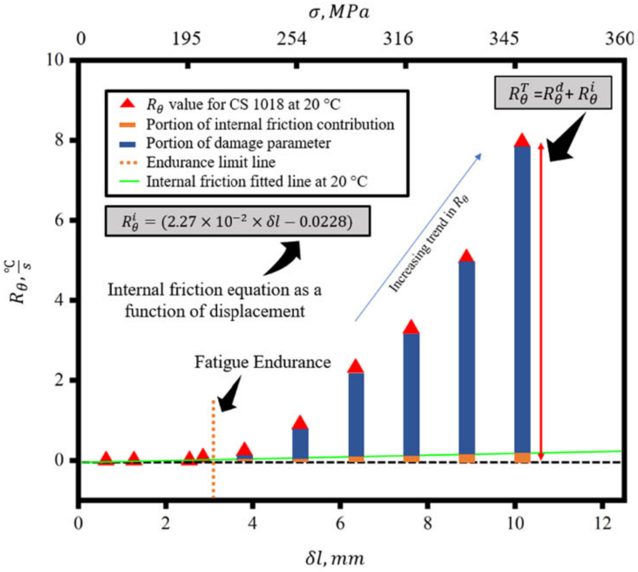

Fig. 10. Internal friction contribution in R_θ^T as a function of displacement at 293 K.

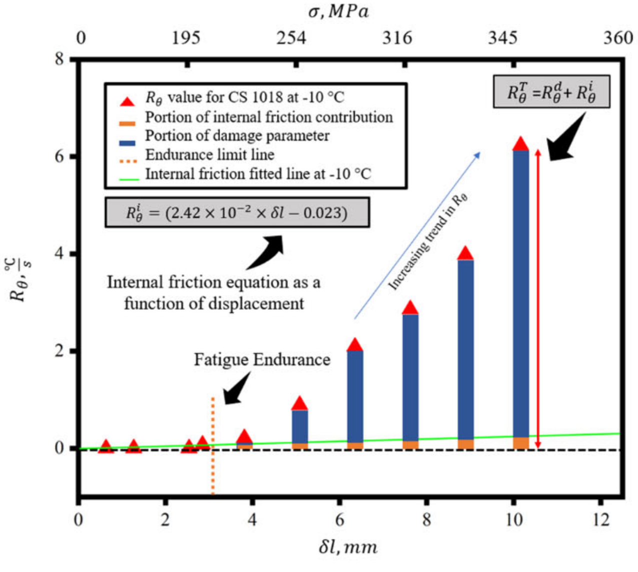

Fig. 11. Internal friction contribution in R_θ^T as a function of displacement at 263 K.

Fig. 12 shows variations in steady-state temperature compared to the initial temperature. This figure shows the proportionality of change in environmental temperature and steady-state temperature and the connection with internal energy changes, as the ΔT for tested temperatures are close. Fig. 13 shows the energy generation caused by the internal friction per cycle at ambient and low temperatures. It shows that the amount of dissipated energy by internal friction in low temperatures is more significant than that of the ambient temperature and this difference increases with an increase in stress levels. It should be noted the diagram shows the rate per cycle. In high-cycle tests, the role of internal friction in energy dissipation becomes more pronounced.

5.2. Fracture fatigue entropy

Fig. 14 shows the FFE values calculated using equations (16) and (17) after subtracting the contribution of internal friction. The FFE changes within a smaller band and varies between 19.7 and 24.2. The FFE range is calculated to remain in the band of 23 ± 2.25 MJ/m^{3}K.

The S-N curves for CS 1018 at four tested temperatures, along with the curve-fitted equations are presented in Fig. 15.

6. Application

This section is devoted to examining the application of FFE in predicting fatigue life in both ambient and lower temperatures. Two specimens are mounted on the machine and the tests are conducted at two different temperatures. Both specimens are undergoing the same amount of stress set to 320 MPa (corresponding to 8.255 mm displacement amplitude). The first test (Test a) is conducted at room temperature (20 °C) and Test b is done at a low temperature of −10 °C. Parameters calculated based on the experimental data are summarized below.

The data based on the S-N curve shows that the life for ambient and low temperatures should be approximately 13,500 and 15,000 cycles, respectively, using the equations $S = 1120.40N_f^{-0.1303}$ for low temperature and $S = 961.91N_f^{-0.1157}$ for ambient temperature.

The average FFE for ambient temperature is 23.2 MJ/m^{3}K. Then based on the internal friction equation given in Figs. 10 and 11, effective R_θ^d can be calculated.

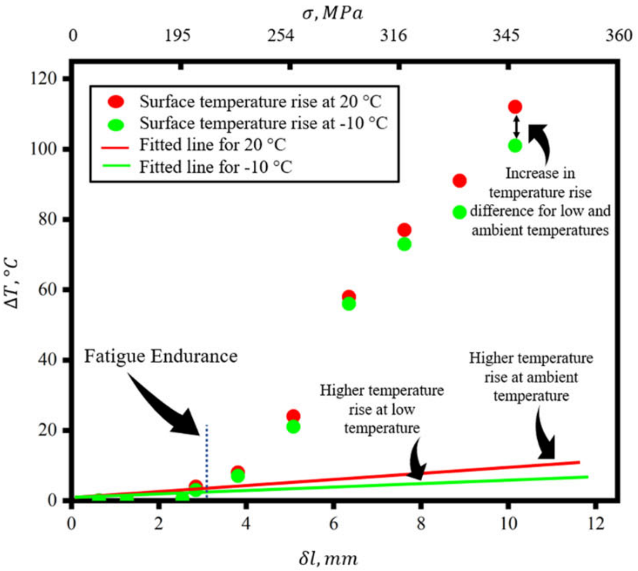

Fig. 12. Temperature rise below and above fatigue limit for both 293 K and 263 K.

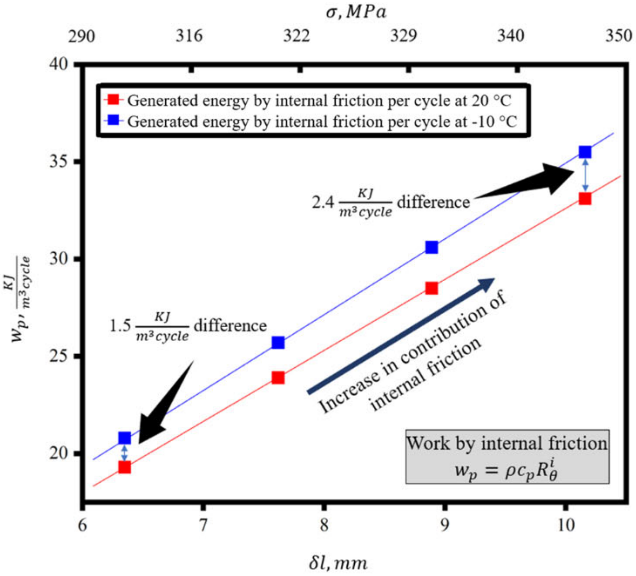

Fig. 13. Energy generation variation by internal friction for different displacements at two temperatures.

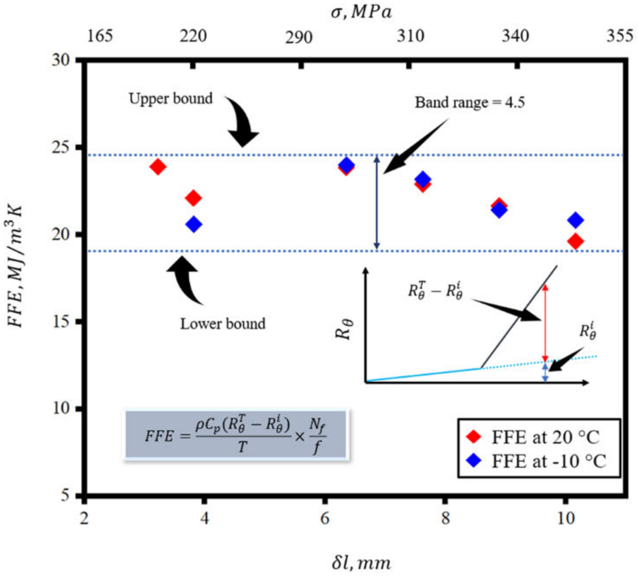

Fig. 14. Calculated FFEs for CS 1018 at 10 °C and 20 °C with consideration of internal friction.

$$R_\theta^i = \left(2.27\times10^{-2}\times\delta l - 0.0228\right)$$
$$\rightarrow R_\theta^i = \left(2.27\times10^{-2}\times8.225 - 0.0228\right) = 0.16\ ^\circ\mathrm{C/s}$$

$$R_\theta^d = R_\theta^T - R_\theta^i = 4.31 - 0.16 = 4.15\ ^\circ\mathrm{C/s}$$

Now with having damaging slope (R_θ^d), the FFE equation can be used to get the life.

$$\mathrm{FFE} = \frac{\rho C_p R_\theta^d}{T}\times\frac{N_f}{f}$$
$$\rightarrow N_f = \frac{\mathrm{FFE}\times T\times f}{\rho C_p R_\theta^d} = \frac{23.2\times379\times24}{7.86\times0.486\times4.15}\approx 13,311$$

The same procedure is carried out for −10 °C. First, the internal friction contribution on the initial temperature slope is calculated and deducted from the overall initial slope. Considering the damaging

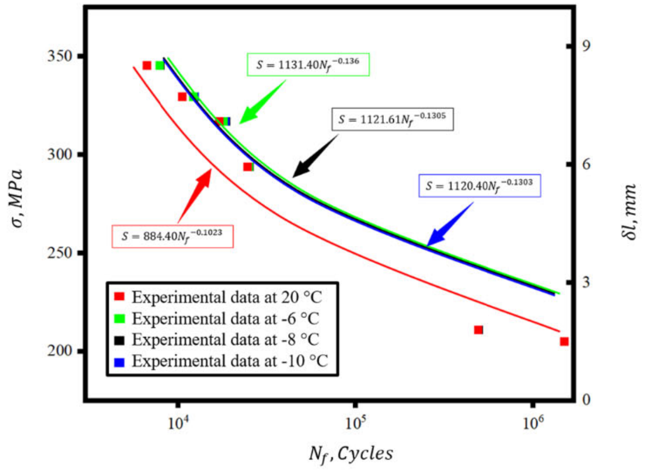

Fig. 15. S-N curves for CS 1018 at 4 various environmental temperatures.

element of the initial slope, the life can be calculated as follows using FFE.

$$R_0^i = \left(2.42 \times 10^{-2} \times \delta l - 0.023\right)$$
$$\rightarrow R_0^i = \left(2.42 \times 10^{-2} \times 8.225 - 0.023\right) = 0.17^{\circ}\mathrm{C/s}$$

$$R_0^d = R_0^T - R_0^i = 3.45 - 0.17 = 3.28^{\circ}\mathrm{C/s}$$

$$\mathrm{FFE} = \frac{\rho C_p R_0^d}{T} \times \frac{N_f}{f}$$
$$\rightarrow N_f = \frac{\mathrm{FFE} \times T \times f}{\rho C_p R_0^d} = \frac{23.2 \times 341 \times 24}{7.86 \times 0.486 \times 3.28} \approx 15,153$$

To validate the predictions, two tests were conducted with the same amount of stress and displacement amplitude at two ambient and low temperatures to validate the data calculated using FFE and S-N curves. The life for ambient temperature is 13,660 and for low temperature is 15,970, which shows 2.62 % and 5.39 % error with those calculated using FFE, respectively.

7. Conclusions

An experimental study was conducted on the fatigue life dependency of CS 1018 on environmental temperatures varying from 20 °C to −10 °C. Of particular interest is to determine the applicability of FFE for various environmental conditions. Internal friction as a non-damaging parameter in fatigue was taken into account and the effect of low temperatures in changing this element has been investigated. The findings of this research are summarized below.

- It was observed that life improves by reducing the environmental temperatures ranging from 20 °C to −10 °C for CS 1018. The life improvement was shown to be a function of temperature and the imposed stress level.
- Dissipated energy during the fatigue process was measured for different temperatures varying from 20 °C and −10 °C and it is shown that CS 1018 experiences less energy dissipation per cycle at lower temperatures. However, the accumulated dissipated energy is larger at lower temperatures. Internal friction, as a non-damaging parameter, is more significant at lower temperatures down to −10 °C.
- Fatigue endurance does not change significantly with a temperature drop in the studied range.
- It is shown that FFE remains constant at low ambient environmental temperatures down to −10 °C. For CS1018, FFE = 23 ± 2.25 MJ/m^3 K.
- The S-N curve and FFE results, compared to experimental validations, showed good reliability for predicting life at various temperatures.

Declaration of Competing Interest

The authors declare that they have no known competing financial interests or personal relationships that could have appeared to influence the work reported in this paper.

Data availability

Data will be made available on request.

Acknowledgments

This research was supported in part by the members of the NSF Center for Innovations in Structural Integrity (CISIA) (Award number 2052810). The authors gratefully acknowledge the support of this research.

References

[1] Jirandehi AP, Khonsari MM. General quantification of fatigue damage with provision for microstructure: a review. Fatigue Fract Eng Mater Struct 2021;44(8):1973–99.
[2] Ghadimi H, Jirandehi AP, Nemati S, Guo S. Small-sized specimen design with the provision for high-frequency bending-fatigue testing. Fatigue Fract Eng Mater Struct 2021;44(12):3517–37.
[3] Ye XW, Su YH, Han JP. A state-of-the-art review on fatigue life assessment of steel bridges. Math Probl Eng 2014;2014:1–13.
[4] Jirandehi AP, Khonsari M, Guo S, Gradl P. Fatigue assessment of additively-manufactured C-18150 copper alloy at room and elevated temperatures via a microstructure-sensitive algorithm. Int J Fatigue 2022;159:106777.
[5] McCammon R, Rosenberg H. The fatigue and ultimate tensile strengths of metals between 4· 2 and 293° K. In: Proceedings of the Royal Society of London. Series A. Mathematical and Physical Sciences, vol. 242, no. 1229, pp. 203-211, 1957.
[6] Stephens R, Chung J, Glinka G. Low temperature fatigue behavior of steels—A review. SAE Trans 1979:1892–904.
[7] Verkin B, Grinberg N, Serdyuk V, Yakovenko L. Low temperature fatigue fracture of metals and alloys. Mater Sci Eng 1983;58(2):145–68.
[8] Vogt J, Foct J, Regnard C, Robert G, Dhers J. Low-temperature fatigue of 316L and 316LN austenitic stainless steels. Metall Trans A 1991;22(10):2385–92.
[9] Kang K-W, Goo B-C, Kim J-H, Kim D-K, Kim J-K. Experimental investigation on static and fatigue behavior of welded SM490A steel under low temperature. Int J Steel Struct 2009;9(1):85–91.
[10] Fassina P, Brunella MF, Lazzari L, Re G, Vergani L, Sciuccati A. Effect of hydrogen and low temperature on fatigue crack growth of pipeline steels. Eng Fract Mech 2013;103:10–25.
[11] Jung D-H, Kwon J-K, Woo N-S, Kim Y-J, Goto M, Kim S. S–N fatigue and fatigue crack propagation behaviors of X80 steel at room and low temperatures. Metall Mater Trans A 2014;45(2):654–62.
[12] Liao X, Wang Y, Qian X, Shi Y. Fatigue crack propagation for Q345qD bridge steel and its butt welds at low temperatures. Fatigue Fract Eng Mater Struct 2018;41(3):675–87.
[13] Zhang D, Li Z, Wu H, Huang F. Experimental study on fatigue behavior of Q420 high-strength steel at low temperatures. J Constr Steel Res 2018;145:116–27.
[14] Khonsari MM, Amiri M. Introduction to thermodynamics of mechanical fatigue. CRC Press; 2012.
[15] Naderi M, Amiri M, Khonsari M. “On the thermodynamic entropy of fatigue fracture. *Proc Roy Soc A: Math, Phys Eng Sci,* vol. 466, no. 2114, pp. 423-438, 2010.
[16] Jang J, Khonsari M. Experimentally validated thermodynamic theory of metal fatigue. Mech Mater 2021:103927.
[17] Jirandehi AP, Khonsari M. Microstructure-sensitive estimation of fatigue life using cyclic thermodynamic entropy as an index for metals. Theor Appl Fract Mech 2021;112:102854.
[18] Teng Z, Wu H, Boller C, Starke P. Thermodynamic entropy as a marker of high-cycle fatigue damage accumulation: Example for normalized SAE 1045 steel. Fatigue Fract Eng Mater Struct 2020;43(12):2854–66.
[19] Ontiveros V, Amiri M, Kahirdeh A, Modarres M. Thermodynamic entropy generation in the course of the fatigue crack initiation. Fatigue Fract Eng Mater Struct 2017;40(3):423–34.
[20] Idris R, Abdullah S, Thamburaja P, Omar MZ. Prediction of fatigue crack growth rate based on entropy generation. Entropy 2019;22(1):9.
[21] Huang J, Li C, Liu W. Investigation of internal friction and fracture fatigue entropy of CFRP laminates with various stacking sequences subjected to fatigue loading. Thin-Walled Struct 2020;155:106978.

[22] Wei W, Du L, Zhang Y, Sun Y, Yang X. Fatigue reliability evaluation of Q460 welded joints using fracture fatigue entropy method. Eng Fract Mech 2021;247:107641.

[23] Huang J, Yang H, Liu W, Zhang K, Huang A. Confidence level and reliability analysis of the fatigue life of CFRP laminates predicted based on fracture fatigue entropy. Int J Fatigue 2022;156:106659.

[24] Haghshenas A, Khonsari M. Non-destructive testing and fatigue life prediction at different environmental temperatures. Infrared Phys Technol 2019;96:291–7.

[25] Jang J, Khonsari M. On the evaluation of fracture fatigue entropy. Theor Appl Fract Mech 2018;96:351–61.

[26] Mehdizadeh M, Khonsari M. On the role of internal friction in low-and high-cycle fatigue. Int J Fatigue 2018;114:159–66.

[27] Naderi M, Khonsari M. A thermodynamic approach to fatigue damage accumulation under variable loading. Mater Sci Eng A 2010;527(23):6133–9.

[28] Meneghetti G. Analysis of the fatigue strength of a stainless steel based on the energy dissipation. Int J Fatigue 2007;29(1):81–94.

[29] Mikhail ISG, Blanter S, Hartmut Neuhäuser, Hans-Rainer Sinning, *Internal Friction in Metallic Materials* (Springer Series in Materials Science). Springer Berlin, Heidelberg, 2007. 978-3-540-68758-.

[30] Huang Z, Liu H, Wang C, Wang Q. Fatigue life dispersion and thermal dissipation investigations for titanium alloy TC17 in very high cycle regime. Fatigue Fract Eng Mater Struct 2015;38(11):1285–93.

[31] Sabar H, Berveiller M, Favier V, Berbenni S. A new class of micro–macro models for elastic–viscoplastic heterogeneous materials. Int J Solids Struct 2002;39(12):3257–76.

[32] Guo Q, Guo X, Fan J, Syed R, Wu C. An energy method for rapid evaluation of high-cycle fatigue parameters based on intrinsic dissipation. Int J Fatigue 2015;80:136–44.

[33] Mehdizadeh M, Haghshenas A, Khonsari M. On the effect of internal friction on torsional and axial cyclic loading. Int J Fatigue 2021;145:106113.

[34] Jhansale H, Topper T. Engineering analysis of the inelastic stress response of a structural metal under variable cyclic strains. In: *Cyclic Stress-Strain Behavior—Analysis, Experimentation, and Failure Prediction*: ASTM International, 1971.

[35] Schijve J. Fatigue of structures and materials. Springer; 2009.